Intrinsic quantum chaos and spectral fluctuations within the protactinium atom

Pascal Naubereit,[1,*] Dominik Studer,[1] Anna V. Viatkina,[2] Andreas Buchleitner,[3]
Barbara Dietz,[4] Victor V. Flambaum,[2,5] and Klaus Wendt[1]
[1]*Institute of Physics, University of Mainz, 55128 Mainz, Germany*
[2]*Helmholtz Institute, University of Mainz, 55128 Mainz, Germany*
[3]*Physikalisches Institut, Albert-Ludwigs-Universität Freiburg, 79104 Freiburg, Germany*
[4]*School of Physical Science and Technology and Key Laboratory for Magnetism and Magnetic Materials of MOE, Lanzhou University, Lanzhou, Gansu 730000, China*
[5]*School of Physics, University of New South Wales, Sydney 2052, New South Wales, Australia*

(Received 18 May 2018; published 10 August 2018)

Recently, spectroscopic investigations of the protactinium atom applying resonant laser ionization spectroscopy revealed high-resolution data of the single-excitation spectrum of protactinium, reaching slightly beyond the first ionization potential [P. Naubereit *et al.*, preceding paper, Phys. Rev. A **98**, 022505 (2018)]. The more than 1500 recently detected energy levels contain several complete sequences of levels. In this work we study the spectral fluctuations of these data exhibiting clear signatures of intrinsic quantum chaos within the protactinium atom. In order to obtain an estimate on possibly missing levels, simulations were performed based on large ensembles of random matrices from the Gaussian orthogonal ensemble. Our experimental results show that tabulated data in the literature are far from completeness and atomic structure calculations severely underestimate the density of states in the spectral range of highly excited states. However, the statistical analysis of our data as well as of the data from literature and calculations predict a level statistics close to that of fully developed chaos at energies well below the single-ionization threshold.

DOI: 10.1103/PhysRevA.98.022506

I. INTRODUCTION

As much as classical systems, like, e.g., the double pendulum, can exhibit a transition from regular to chaotic dynamics, the spectral properties of quantum systems can change drastically [1]. This is well established by now both theoretically and experimentally for few-degrees-of-freedom systems [2–11]. In contrast, evidence for quantum chaos in systems existing on higher-dimensional (classical) phase spaces which also have a much more intricate topology, giving rise, e.g., to Arnold diffusion [12–15], and likely are at the origin of many-body localization [16,17], is rather scarce, with only a few systematic results [18–24] so far. This fact is due to the unfavorable scaling properties of the density of states with increasing excitation energy, accompanied by strong coupling between the various degrees of freedom. On the theoretical as well as on the experimental side, this defines substantial challenges for the resolution of the relevant spectral structures [7]. Atomic many-body systems constitute ideal, naturally occurring test cases for such proliferation of complexity, where the generic presumption holds that the chaotic proportion of phase space increases with the excitation energy, while an unambiguous designation of the demarcation line between regularity and chaos has so far remained elusive [15,20,25–27]. In truly complex many-body systems, e.g., an actinide atom, the transition point from regularity to significant chaoticity is expected already at low excitation energies. A proof is pending, because complete high-resolution spectroscopic data from the ground state up to the first-ionization potential were and still are unavailable. Even for lighter elements, very few cases of investigation of intrinsic quantum chaos (IQC), meaning without outer influence of artificially applied electromagnetic fields or scattering processes by specific projectiles, in complex atomic systems are available [28–30].

Here we analyze spectral fluctuation properties in the recent spectroscopic data collected for protactinium and presented in Ref. [31] using as statistical measures the nearest-neighbor spacing distribution (NNSD), the number variance Σ^2, and the spectral rigidity Δ_3. For further explanations see Sec. II. According to the Bohigas-Giannoni-Schmit conjecture [32], the spectral fluctuation properties are universal and coincide with those of uncorrelated random numbers exhibiting Poisson statistics for classically integrable systems and with those of random matrices from the Gaussian orthogonal ensemble (GOE) if the classical dynamics is fully chaotic. For a proper analysis we have to deal with problems stemming primarily from missing or spurious levels. Therefore, large ensembles of random matrices from the GOE were generated and a certain fraction of eigenvalues was randomly deleted in order to simulate missing levels. The resulting statistics are compared to the experimental data.

Recently [31], about 1500 hitherto unknown resonances were detected in the bound spectrum of the Pa atom, covering selected energy ranges, different total angular momentum states, and both parities have been tabulated. An exemplary spectrum, corresponding to scheme (iii) of [31], is shown in the top panel of Fig. 1, covering excitation energies from below

*naubereit@uni-mainz.de

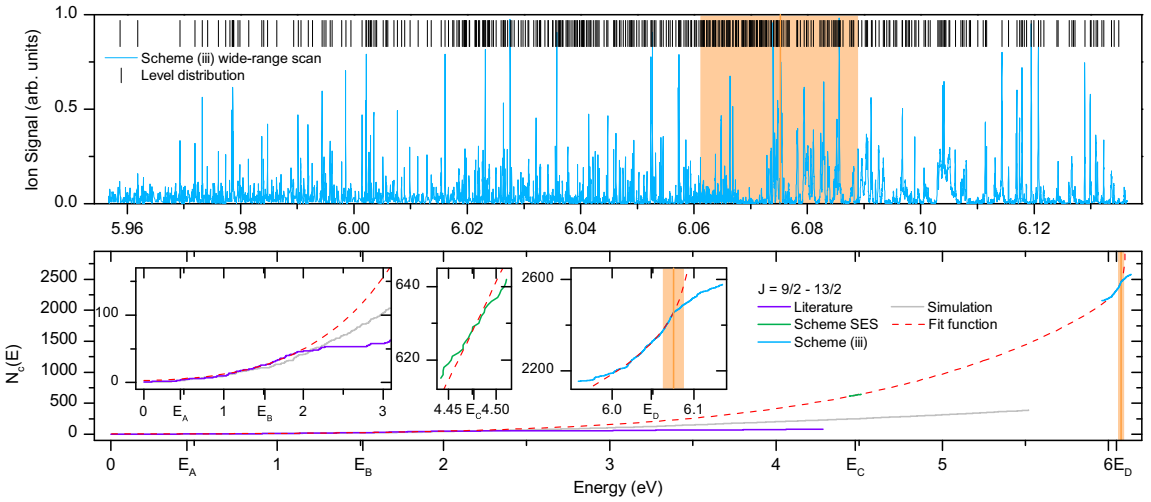

FIG. 1. The top graph shows the highly resolved excitation spectrum of protactinium for excitation scheme (iii) of [31], complemented by the corresponding level distribution (black lines above spectrum). The bottom graph shows the staircase functions for the cumulative number of resonances, as inferred from the literature (purple) [33], simulation (light gray) [34], and the present experimental data sets (green and blue) around E_C and E_D, respectively. The dashed red line represents the self-consistent fit to the spectral density over the entire energy range; see the main text for details. The orange vertical line in all plots indicates the estimated ionization potential, with its uncertainty range identified by the orange-shaded region [35]. For further explanations also on the three insets, see the text.

to slightly above the first ionization potential. The data of [31] serve as a basis for the analysis of intrinsic quantum chaos and its spectral characteristics in this highly complex atomic system.

II. LEVEL STATISTICS AND LEVEL DENSITY FLUCTUATIONS

A. Level density in general

Let us first compare the density of states of the experimental data, the available literature, and simulation data. The bottom panel of Fig. 1, together with the insets which zoom into three selected energy ranges, shows the cumulated number of energy levels

$$N_c(E) = \int_0^E \sum_i \delta(E' - E_i) dE' \tag{1}$$

as a staircase function of the excitation energy, with E_i the energy of the ith resonance. As explained in Ref. [31], our experimental data are limited to a range of three subsequent total angular momenta. Therefore, we took into account in the analysis of the simulated and the literature data only energy levels with $J = \frac{9}{2}, \ldots, \frac{13}{2}$. The apparent significant decrease of the level density just above the first ionization potential, as evident in the rightmost inset, can be explained by our experimental method: While resonances in the continuum still may bind all five electrons, many of these resonances are hidden by a continuum background due to broad autoionizing or ionic resonances, which becomes manifest in the top panel of Fig. 1 as a clearly visible broadening of the resonances above approximately 6.07 eV. This behavior was generally observed for all scans reaching beyond the expectation value of the ionization potential. A second reason is the termination of various Rydberg series converging towards the ionization potential.

For the simulation data, a loss of accuracy and completeness is anticipated already well below threshold, because only low-energy configurations had so far been included in these calculations [34]. In addition, the model neglects correlations between core and valence electrons, which are known to contribute substantially at higher excitation energies. Consequently, the experimental staircase function is expected to grow faster than the one predicted by the simulation, which exhibits an approximately quadratic energy dependence (see the gray line in the leftmost inset of the bottom panel of Fig. 1).

In order to compare the level densities of the experimental data [31] with those of the literature and simulation data and to localize strong deviations between them we performed a fit of $N_c^{\mathrm{tot}}(E)$ to the overall experimental density using the prediction for its average

$$\frac{d}{dE} N_c'(E) = \rho_0 e^{a\sqrt{E}} \tag{2}$$

for the density of states of an interacting many-body spectrum [29], which neglects Rydberg excitations of either one of the electrons. Thus, in the ansatz for $N_c^{\mathrm{tot}}(E)$, a phenomenological Rydberg term is included:

$$N_c^{\mathrm{tot}}(E) = N_c'(E, \rho_0, a) + r\sqrt{\frac{hcR}{E_{\mathrm{IP}} - E}}. \tag{3}$$

Here hcR is the mass-reduced Rydberg energy and ρ_0, a, r, and E_{IP} are free fitting parameters, where r could be interpreted as the number of Rydberg series involved and E_{IP} as the ionization potential. This procedure is legitimate since no chaotic perturbation is expected for high principal quantum numbers of single-electron Rydberg levels according to [36]. However, the data sets of scans in the energy range between 4.48 and 6.05 eV, denoted by SES (for second excitation step) and (iii), which are exemplarily considered from [31] and shown in the middle and right insets of the bottom panel

of Fig. 1, provide no information on how many levels lie below and between these associated energy ranges. To extract a consistent offset for the disjoint data sets, we fit $\partial N_c^{\mathrm{tot}}(E)/\partial E$ to the slopes of the cumulated density of states, as visualized in Fig. 1, within four predefined energy intervals E_A, E_B, E_C, and E_D, centered around the excitation energies 0.46, 1.52, 4.48, and 6.05 eV, respectively. These regions most optimally incorporate the different available data sets, stemming either from the literature at low excitation energies (E_A and E_B, where only the three J values studied in the experiment are accounted for) or from the experimental data of [31] at medium or high excitation energies (E_C and E_D). By this procedure, initially the offsets of the SES and (iii) scans were determined and the specific subsets of the three different data sets depicted in the three insets, now properly leveled, were fitted by $N_c^{\mathrm{fit}}(E)$. The resulting fitting parameters are reasonable: A value of $r = 16(6)$ for the different involved Rydberg series is realistic and $E_{\mathrm{IP}} = 6.11(1)$ eV matches the estimate of 6.075(14) eV for the ionization potential derived from systematics [35].

The resulting curve for the overall level density is shown as a red dashed line in the bottom panel of Fig. 1 as well as in the close-ups of the three insets. The comparison to the experimental data reveals three remarkable facts.

(a) The theoretical simulations, which only incorporate low-energy configurations, give correct and complete level densities up to excitation energies around 1.5 eV and slowly start to deviate at higher energies.

(b) Literature data appear to be complete up to energies around 2 eV, with a sharp cutoff at this value.

(c) The experimental data taken around E_C and E_D are well matched by the fit. Both data sets thus confirm the completeness of the levels detected in these energy ranges.

The issue of missing levels will be addressed Sec. III. Here "completeness" refers to unexpected deviations of the level density from its energy-dependent average, for example visible in the bottom panel of Fig. 1 for the literature data above 2 eV or for scheme (iii) above 6.07 eV. The slight deviations observed at the edges of both data sets (middle and right inset) are ascribed to a signal depletion at the edges of our laser scan ranges, due to decreasing laser power, as well as to the emerging continuum background discussed above for the energy range beyond the ionization threshold. Therefore, only the following parts of the individual data sets were employed in our subsequent analysis: For the even literature data a range of $0.00, \ldots, 2.00$ eV, for the SES scheme a range of $4.44, \ldots, 4.51$ eV, and for scheme (iii) a range of $5.96, \ldots, 6.08$ eV were evaluated.

B. Nearest-neighbor spacing distribution

Based on the above confirmation of the essential completeness of our experimental spectra in the inspected energy intervals, we can now proceed towards an analysis of the spectral structure of protactinium in terms of statistical measures commonly used in random matrix theory (RMT). We extract the nearest-neighbor spacing distribution, as one of the fundamental quantifiers of regularity-to-chaos transition in complex quantum systems [37], as area-normalized histograms of normalized, dimensionless energy spacings

$$s_i = \xi_{i+1} - \xi_i, \tag{4}$$

with the unfolded energy

$$\xi_i = N_c^{\mathrm{fit}}(E_i), \tag{5}$$

obtained by utilizing the smooth part of the staircase function, i.e., its fit function $N_c^{\mathrm{fit}}(E)$ [38]. Second-order polynomials serve as fit functions for the unfolding of all experimental level sets as well as of the numerically simulated spectral data from [34].

Random matrix theory predicts a Poisson distribution

$$P_{\mathrm{P}}(s) = e^{-s} \tag{6}$$

for the individual s_i in the limit of regular spectra, i.e., in systems of well-preserved quantum numbers, and a Wigner-Dyson distribution [39]

$$P_{\mathrm{WD}}(s) = \frac{\pi}{2} s e^{-(\pi/4)s^2} \tag{7}$$

in the limit of fully broken integrability, synonymous with the complete destruction of good quantum numbers, within subspaces defined by one specific value J of the total angular momentum [37]. Both these idealized limits are interpolated by the Brody distribution

$$P_{\mathrm{B}}(s,\eta) = a s^{\eta} e^{-b s^{\eta+1}}, \quad a = (\eta+1)b, \quad b = \Gamma\left(\frac{\eta+2}{\eta+1}\right)^{\eta+1}, \tag{8}$$

with Euler's Gamma function Γ. The Brody parameter η controls this interpolation, with the limiting cases $\eta = 0$ for the Poisson and $\eta = 1$ for the Wigner-Dyson distribution [40].

Since our experimental spectra are superpositions of three independent J manifolds, we furthermore need to account for the thereby induced convolution of distinct distributions. This can be achieved with the help of the superposition formula initially suggested by Rosenzweig and Porter [28]. Here we utilize Eq. (3.69) from [38], giving the spacing distribution $P_{3\mathrm{B}}(s,\eta)$ for superpositions of three independent subspectra. In doing so, we make two assumptions.

(i) The level density in all three J manifolds is equal.

(ii) The manifolds exhibit the same energy dependence of $\eta(E)$.

A comparison with simulation and literature data validates both assumptions as reasonable first-order approximations [33,34]. A second interpolating function applicable to superimposed spectra is the Abul-Magd distribution [24,41]

$$P_{\mathrm{AM}}(s,f) = \left(1 - f + \frac{\pi}{2} Q(f) s\right) e^{-(1-f)s - (\pi/4)Q(f)s^2}, \tag{9}$$

with $Q(f) = 0.7f + 0.3f^2$. The parameter f of this description similarly approaches the Poisson distribution for $f \to 0$ and the Wigner-Dyson distribution for $f \to 1$, but the meaning is different as for the superposition of three Brody distributions: While the η parameter of the Brody convolution gives a hint at a close-to-GOE behavior of the three independent subspectra, the f parameter expresses a prediction for the number of superimposed fully chaotic GOE spectra. Thus, the number of independent GOE subspectra is given by $n = \frac{1}{f}$.

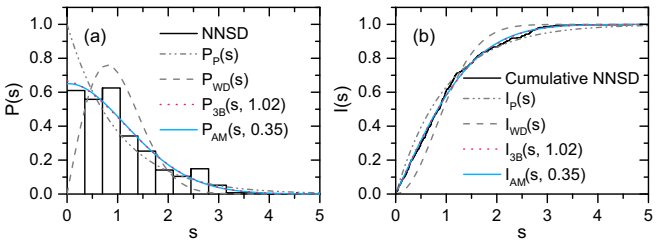

FIG. 2. (a) Nearest-neighbor spacing distribution $P(s)$ and (b) corresponding cumulative NNSD $I(s)$ for simulated data with $J = \frac{9}{2}, \ldots, \frac{13}{2}$. The Poisson and Wigner-Dyson distributions are shown as gray dash-dotted and dashed lines, respectively. The fitted Abul-Magd distribution is displayed as a blue line and the convoluted Brody distribution as a dotted red line.

The special case of three superimposed subspectra yields $P_{3B}(s, 1) \equiv P_{AM}(s, \frac{1}{3})$.

To determine the best-fit Brody parameter η or Abul-Magd parameter f, the maximum-likelihood (MLH) method [42] was used. This method is, in contrast to a least-squares-fitting method, completely independent from the binning procedure, since it is directly applied to the raw data. The uncertainty of η and f is conservatively approximated by the half-width at half maximum (HWHM) of the likelihood distribution.

Figure 2(a) shows an exemplary NNSD. Especially for small spacings and/or a small number of spacings, the cumulative nearest-neighbor spacing distribution (CNNSD)

$$I(s) = \int_0^s P(s')ds' \tag{10}$$

is more reliable for comparing the fits with the data. In Fig. 2(b) the CNNSD is shown. The NNSD is obtained from the simulated data with superimposed subspectra with $J = \frac{9}{2}, \ldots, \frac{13}{2}$. Besides the two fitted distributions P_{3B} and P_{AM} for the NNSD and I_{3B} and I_{AM} for the CNNSD, the curves for Poisson (P_P and I_P) and Wigner-Dyson (P_{WD} and I_{WD}) distributions are indicated as gray dash-dotted and dashed lines, respectively. The histograms are depicted for illustration; however, they were not used for the fitting procedure. The NNSD and CNNSD for the simulated data show a level repulsion close to that of chaotic GOE spectra. Both repulsion parameters $\eta = 1.02(30)$ and $f = 0.35(14)$ match the expected values of $\eta = 1$ and $f = \frac{1}{3}$, respectively, for a convolution of three GOE spectra very well. The rather large uncertainties of these values are caused by a broad likelihood distribution because the convoluted Brody distribution and the Abul-Magd distribution barely change in their shapes when varying the parameters η and f around a given value.

For an estimation of the quality of the fits for the CNNSD, the residuals $I_{3B} - I(s)$ and $I_{AM} - I(s)$ are shown in Fig. 3 as the difference between the resulting fit curves and the data. This form of presentation gives an idea of the shape of the NNSD and CNNSD by regarding the distribution parameters η and f and therefore a hint of the chaotic repulsion of the neighboring energy levels. In addition, it provides information on the quality of the individual fits of the CNNSD. Thus, in the following analysis only these residuals will be discussed when analyzing the level repulsion in the experimental data sets as short-range correlation.

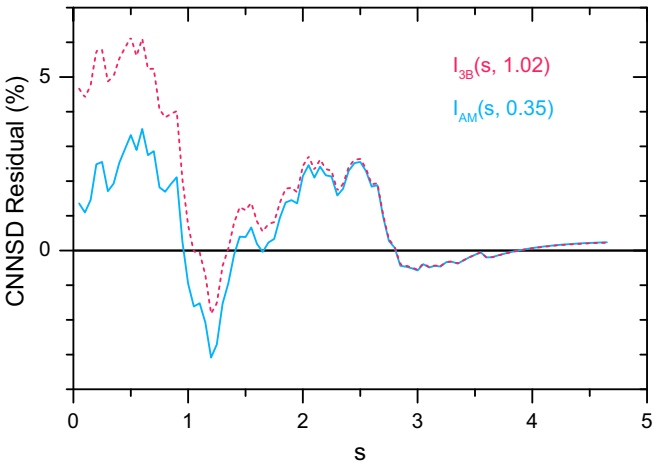

FIG. 3. Residuals of the fitted curves for the CNNSD. Here $I_{3B} - I(s)$ is given as a dotted red line and $I_{AM} - I(s)$ as a blue solid line.

For the experimental data, the NNSDs are conclusive only after accounting for missing levels. Because of that, we proceed similarly in the following two sections about the statistical measure's number variance and spectral rigidity and explain them by means of the simulated data first. The experimental measurements will be discussed afterward in detail in Sec. IV involving all statistical measures.

C. Number variance $\Sigma^2(L)$

The NNSD gives information on the repulsion of energy levels and shows correlations on the shortest possible scale, namely, on the scale of one or two mean spacings. Accordingly, the NNSD is sensitive with respect to the unfolding procedure, missing levels and the fitting procedure used for its description, however, by far not as sensitive as long-range correlations. Thus the NNSD itself does not serve as a significant measure for GOE or Poisson behavior. One additional measure for spectral statistics, which gives information on long-range correlations, is given by the variance $\Sigma^2(L)$ of the number $\nu(L)$ of unfolded levels in an interval with length L [38],

$$\Sigma^2(L) = \langle \nu^2(L) \rangle - \langle \nu(L) \rangle^2. \tag{11}$$

Here the angular brackets stand for a spectral average. Like a variance in stochastics, also the quantity $\Sigma^2(L)$ gives the mean-square deviation of the number of energy levels in an interval L from their mean L. For uncorrelated Poissonian spectra, $\Sigma^2_P(L)$ grows linearly with the correlation length L. For highly correlated GOE spectra, the variance $\Sigma^2_{GOE}(L)$ grows slower according to a logarithmic slope for large L. For our case of three superimposed subspectra, the spectral correlation is lower as in the GOE case. The resulting curve for $\Sigma^2_{3GOE}(L)$ can easily be calculated [38]:

$$\Sigma^2_{3GOE}(L) = \sum_{m=1}^{3} \Sigma^2_{GOE}\left(\frac{L}{3}\right). \tag{12}$$

Figure 4(a) shows the level number variance for the simulated data with $J = \frac{9}{2}, \ldots, \frac{13}{2}$ and the theoretical curves for the cases of Poissonian statistics, GOE statistics, and the statistics of three convoluted GOE spectra. The data matches the expected

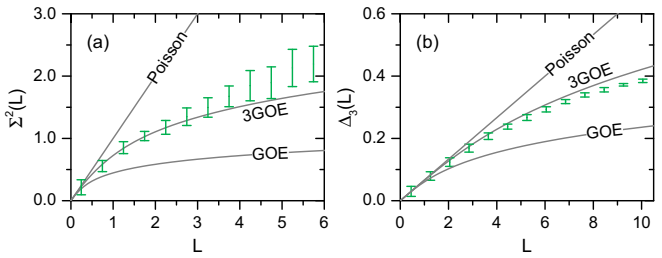

FIG. 4. (a) Number variance $\Sigma^2(L)$ and (b) spectral rigidity $\Delta^3(L)$ for the simulated data with $J = \frac{9}{2}, \ldots, \frac{13}{2}$. The error bars display the standard deviation of the binning process. The theory curves for Poissonian, GOE, and 3GOE statistics are given as gray lines.

curve for three superimposed GOE spectra (3GOE) perfectly up to a correlation length of $L \leqslant 3.5$. Only for higher L, the data points gradually start to deviate from the theoretical expectation of 3GOE, but still are significantly off from the Poissonian curve. This finding can be interpreted as GOE-like statistics for each of the involved J subspectra as already predicted in [34]. Nevertheless, another observable for long-range correlation statistics, the spectral rigidity $\Delta_3(L)$, will be investigated as a further preparation step for the data analysis presented in Sec. IV.

D. Spectral rigidity $\Delta_3(L)$

The spectral rigidity or Dyson-Metha statistic $\Delta_3(L)$ is defined as the least-squares deviation of the *unfolded* staircase function $\nu(\xi)$ from the best linear fit. Note that after proper unfolding the smooth part of the staircase function is by definition a straight line. The spectral rigidity $\Delta_3(L)$ is given as

$$\Delta_3(L) = \frac{1}{L}\left\langle \min_{A,B} \int_{\xi_s}^{\xi_s+L} [\nu'(\xi) - A\xi - B]^2 d\xi \right\rangle, \qquad (13)$$

where ξ_s defines the first unfolded level energy of an interval of length L [38,39]. Due to its definition, the spectral rigidity is comparable to a χ^2 depending on the correlation length L. Since Δ_3 is rather similar to Σ^2, the spectral rigidity can also be expressed as an integral transform of the number variance [38]

$$\Delta_3(L) = \frac{2}{L^4}\int_0^L (L^3 - 2L^2 r + r^3)\Sigma^2(r)dr. \qquad (14)$$

Similar to the number variance, for the Poissonian case of noncorrelated spectra (14) also leads to a linear expression of $\Delta_3^{\mathrm{P}}(L) = \frac{L}{15}$, while $\Delta_3^{\mathrm{GOE}}(L)$ for correlated GOE spectra again follows a logarithmic trend for large L. The resulting curve for three superimposed GOE spectra is simply calculated in analogy to Eq. (12) by [38]

$$\Delta_3^{\mathrm{3GOE}}(L) = \sum_{m=1}^{3} \Delta_3^{\mathrm{GOE}}\left(\frac{L}{3}\right). \qquad (15)$$

Figure 4(b) shows the spectral rigidity for the three superimposed simulated subspectra with $J = \frac{9}{2}, \ldots, \frac{13}{2}$ as well as the theory curves for Poisson, GOE, and convoluted GOE statistics. The rather small error bars again stem from the standard deviations of each bin. Like the number variance, also the spectral rigidity confirms chaotic GOE behavior of the simulated data for every involved J subset. The data fit the expected theory curve up to correlation lengths of $L \leqslant 5$ and start to slightly deviate above.

As described earlier in this section, the spectral rigidity is calculated from the number variance, which makes both quantities very similar by definition. Therefore, and because of its more smooth character due to the "smoothing" integral transform in Eq. (14), only $\Delta_3(L)$ will be utilized as a measure for long-range correlations of the energy levels in the following analysis of the experimental data.

III. MISSING LEVELS

For an accurate analysis of the experimental data sets it is mandatory to take into account the possibility of missing levels leading to incomplete spectra. The incompleteness of a spectrum will influence the spectral statistics leading to either more GOE-like or more Poissonian-like behavior. Imagine levels are "overlooked" due to the obviously finite spectral resolution of the experiment, where two or more levels may overlap, especially with increasing level density. Also resonances with intensities below the detection threshold may be missed. If levels are randomly extracted from the spectra, all statistical measures for the spectral properties of such incomplete spectra will show a displacement towards Poissonian statistics, simply because the correlation between levels is decreased. In our experiment, which utilizes resonance ionization spectroscopy, such situations cannot be avoided. In addition, especially as three J submanifolds are superimposed, the strength for transitions in subspectra of one specific J value might be significantly suppressed compared to the others. This causes the missing of levels in the respective J submanifold. In this case, the fluctuation properties would exhibit a displacement towards GOE-like behavior for every subspectrum, if the complete spectra exhibit GOE, because the correlations in each independent subspectrum seem to be higher if levels from only one J submanifold are missing. One possible method for characterizing the consequences for a certain number of missing levels in the experimental data is to randomly delete a specific percentage of levels from a set of levels from which we know that it shows GOE statistics.

A. Random matrices

The members of the Gaussian orthogonal ensemble are real symmetric matrices with Gaussian-distributed entries that are invariant under real orthogonal transformations [43]. We generated such matrices with dimension $N = 300$. In order to simulate the experimental situation, where the level sequences are composed of three independent subspectra corresponding to different values of J, we merged the eigenvalues of three random matrices into one sequence before applying the unfolding procedure. In order to improve the statistical significance we considered ensembles composed of five such sequences, thus yielding a set of 4500 levels.

Figure 5 shows the statistical measure for long-range correlation $\Delta_3(L)$ as well as the residuals from fitting the CNNSD with the convolution of three Brody functions and

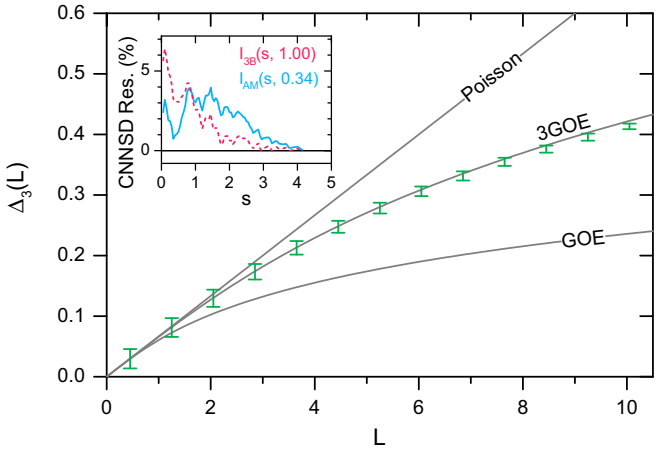

FIG. 5. Spectral rigidity for the RMT eigenvalues. The error bars display the standard deviation of the binning process. The theory curves for Poissonian, GOE, and 3GOE statistics are given as gray lines. The inset comprises the residuals of the CNNSD for the fitted Brody convolution (red dashed line) and the fitted Abul-Magd distribution (blue solid line).

the Abul-Magd distribution for this set of eigenvalues. In the inset of Fig. 5, a Brody parameter of $\eta = 1.00(23)$ and an Abul-Magd parameter of $f = 0.34(4)$ illustrate the expected repulsion of the nearest neighbors in a convolution of three GOE spectra. Even though the fits are lying at slightly higher values than the data, the small residuals also confirm the two extracted repulsion parameters and their uncertainties. In addition, the RMT data coincide perfectly with the theoretical results for the spectral rigidity. Thus, the dimension of the random matrices is large enough to ensure good agreement of the numerical simulations with the theoretical results for correlation lengths in ranges relevant for the experimental data.

B. Missing level statistics

As mentioned above, we have to take care of two types of missing levels. First, there may be randomly missing levels regardless of the subset, or in our case of the J value. Second, levels of a specific subset, or synonymous J manifold, might be suppressed at random and thus not detected. There actually exist exact analytical results for incomplete eigenvalue spectra of random matrices from the Gaussian ensembles [44] which can be generalized to the case of a superposition of three independent GOE matrices. However, because of the fact that we here have to deal with the above-mentioned cases of missing levels, the chosen way of using random matrix ensembles is more straightforward. In the following we will focus on the first case. The second case will be analyzed in detail in Sec. III C.

We simulated the first case by removing a specific percentage of randomly chosen levels from the total set of eigenvalues. To match the experimental situation, this has to be done before the unfolding process takes place. We created an ensemble of random matrices which will have slightly differing spectral properties. To extract the universal fluctuation behavior for a specific percentage of missing levels, we analyzed the distributions of the Brody and Abul-Magd parameters deduced

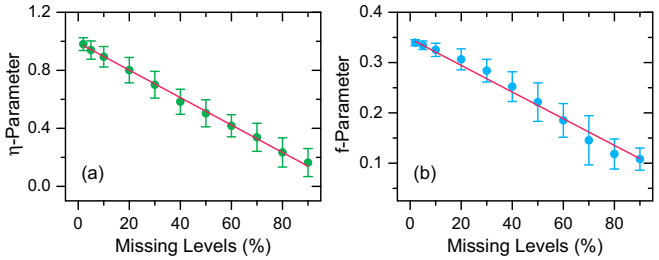

FIG. 6. Dependence of (a) the Brody parameter and (b) the Abul-Magd parameter on the percentage of missing levels regardless of the level subset. For each data point the distribution of the parameters for 100 different level sets has been evaluated. The red lines show linear fits to the data with fit parameters of (a) 0.9902(54) and −0.0095(1) and (b) 0.3474(21) and −0.0027(1) for the intercepts and slopes, respectively.

from fits to the NNSD of 100 level sets for various values of the percentage of missing levels. The resulting distributions are of Gaussian shape and the center positions together with the HWHM values as uncertainties are displayed in Fig. 6 for various percentages of missing levels reaching from 2% to 90%. Both parameters are linearly decreasing as a function of omission percentage. Thus, as expected, the correlations between the remaining neighboring levels are reduced with increasing fraction of missed eigenvalues.

For each fraction of missing levels a representative set of eigenvalues was identified for which a fit of the convoluted Brody and Abul-Magd distributions to the NNSD yields values of η and f as evaluated via Fig. 6. For these data sets also the dependence of the spectral rigidity $\Delta_3(L)$ on the fraction of missing levels has been obtained. Figure 7 shows the spectral rigidity for a choice of percentages of missing levels regardless of their J value, i.e., subset. The plots concerning that type of missing level are labeled with "All J missing." The data for the

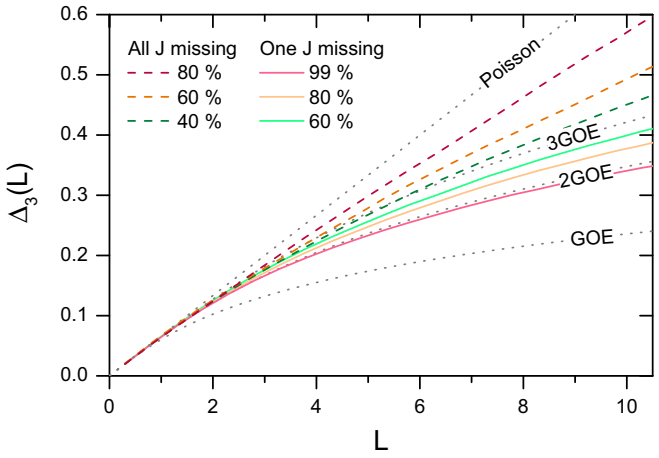

FIG. 7. Spectral rigidity for different percentages of missing levels from all subsets as colored dashed lines with increasing percentages from top to bottom. The colored solid lines represent the spectral rigidity for different percentages of missing levels from one certain subset with increasing percentages from bottom to top. The curves for Poissonian, GOE, 2GOE, and 3GOE behavior are given as gray dotted lines. For more information see the text.

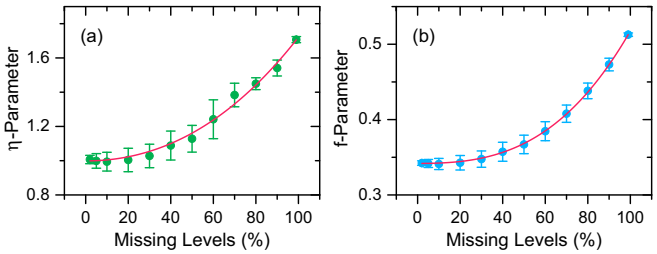

FIG. 8. Dependence of (a) the Brody parameter and (b) the Abul-Magd parameter on the percentage of missing levels in one specific level subset. For each data point the distribution of the parameters for 100 different level sets has been evaluated. The red lines show a cubic fit to the data.

different percentages of missing levels are given as differently colored dashed lines, while the curves for Poissonian and convoluted GOE behavior are given as gray dotted lines. The error bars are omitted in these graphs for the sake of clarity. The remaining graphs will be discussed in Sec. III C. As expected from the features of the NNSDs, the correlations between the remaining levels dwindle the more levels have been taken out, thus the corresponding spectral rigidity approaches the curve for Poissonian statistics accordingly. In contrast to the NNSDs, this approach does not take place in a linear manner: A clear deviation of $\Delta_3(L)$ from the 3GOE curve is observed not before approximately 30% of missing levels, at least within these rather short correlation lengths.

C. *J* suppression

Comparable to the approach in Sec. III B, here also specific amounts of levels are deleted, but now from only one subset in order to simulate the suppression of levels with a specific J value. We proceeded as in Sec. III B and thus obtained for the NNSD parameters a dependence on η and f as illustrated in Fig. 8. Unlike in Fig. 6, here the parameters η and f are well described by a cubic increase with an increasing number of missing levels.[1] Both starting at the values for NNSDs of three convoluted GOE spectra around $\eta = 1$ and $f = \frac{1}{3}$, the parameters remain fairly unchanged until about 30% of missing levels. From this point on the parameters are quickly approaching their final values of $\eta = 1.71(2)$ and $f = 0.51(0.2)$ at 99% missing levels. Of course, a Brody parameter larger than $\eta = 1$ is not very meaningful if a single spectrum is evaluated. Contrarily, it accentuates in our case the increase in level correlation due the reduced influence of one of the independent subsets. Also the Abul-Magd parameter delivers the expected value for a convolution of now only two GOE subspectra with $n = \frac{1}{f} \approx 2$.

Again, representative level sets are found with NNSDs predicted by the distribution of η and f as given in Fig. 8. From these representative sets the spectral rigidity $\Delta_3(L)$ was calculated for several percentages of missing levels. Figure 7 illustrates the results for this type of missing levels as graphs labeled with "One J missing." The theory curves for one, two convoluted, and three convoluted GOE spectra are given together with the curve for the Poissonian case as gray dotted lines. The analyzed data are given as solid lines, differently colored according to the number of missing levels. At first sight it is recognizable that the colored solid lines of Fig. 7 lie between the theory curves of 2GOE and 3GOE. Accordingly, the spectral rigidity $\Delta_3(L)$ shows the expected trend: Starting at the 3GOE curve, it approaches the 2GOE curve where it finally ends up. Note that the curve for 99% missing levels also fully agrees with the 2GOE curve within its uncertainty range, which was omitted here for the sake of clarity. That behavior corresponds to the increase of spectral correlation as seen before in the NNSDs of Fig. 8. Remarkably, $\Delta_3(L)$ does not change very much for percentages of missing levels below 40%–50%, like it was already suggested by the behavior of the NNSD parameters in Fig. 8.

Note that in a spectroscopic experiment, naturally a mixture of both types of missing levels will occur. As described in Secs. III B and III C, either type has a more or less opposite influence on the measures for spectral correlations. Thus, a specific ratio of the occurrence of both types might lead to a compensation of the effects on one of the measures for spectral correlations. Since the effects caused by missing levels are strongly nonlinear for the various statistical measures, we expect that a simultaneous cancellation for all of them is not possible. Hence, in the following analysis of experimental data, always the residuals of the fits for the CNNSD *and* the spectral rigidity are evaluated.

IV. SPECTROSCOPIC DATA

Based upon the statistical measures for spectral fluctuation properties introduced in Sec. II and the results on missing level statistics presented in Sec. III, we can now begin with a detailed analysis of the vast spectroscopic data of the protactinium atom. We will analyze several spectra composed of mainly three subspectra with individual total angular momenta covering different ranges of excitation energy and both parities.

A. Literature data

Data available in the literature [33] cover excitation energies from the ground state at 0 eV up to about 4.5 eV and both parities. We furthermore merged the levels with total angular momenta of $J = \frac{9}{2}, \ldots, \frac{13}{2}$ into one data set. Even-parity levels with an excitation energy above 2 eV have been omitted because of incompleteness indicated by the sharp cutoff observed in Fig. 1 in the left inset. For odd-parity levels we proceeded similarly by also omitting levels for energy ranges where obviously levels are missing according to the level density; in this case levels with excitation energies above 3.7 eV are neglected. Due to the low total count of only 46 energy levels,

[1]Cubic and quadratic fits have been tested, both with an fixed apex at 0% missing levels to guarantee a monotonically increasing function. Because of the worse adjusted R^2 for the quadratic fits of $R^2_\eta = 0.9972$ and $R^2_f = 0.9955$, respectively, in addition to larger residuals in comparison to the cubic fits—here the adjusted R^2 were $R^2_\eta = 0.9975$ and $R^2_f = 0.9999$, respectively—we decided to rely on the cubic fits. We presume that the dependence would be described best by a quadratic function if levels from two subsets, not one or all three, would be taken out. A proof for that conjecture as well as a reason for the found dependences is pending.

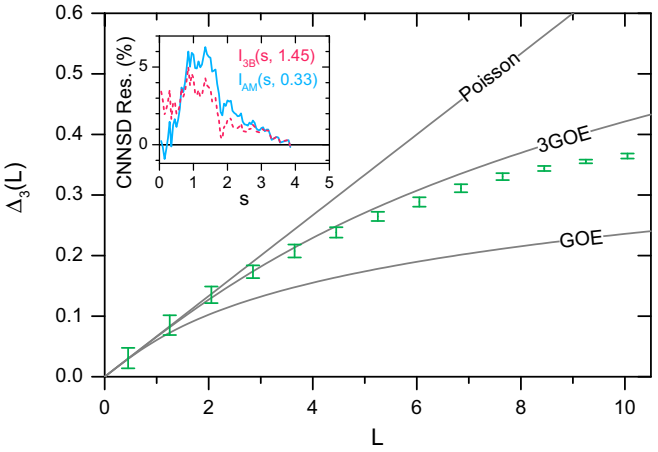

FIG. 9. Spectral rigidity for low-energy odd-parity levels of [33]. The error bars display the standard deviation of the binning process. The theory curves for Poissonian, GOE, and 3GOE statistics are given as gray lines. The inset comprises the residuals of the CNNSD for the fitted Brody convolution (red dashed line) and the fitted Abul-Magd distribution (blue solid line).

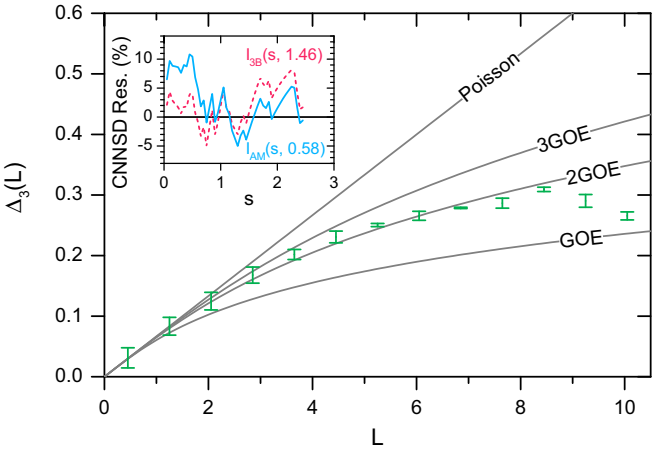

FIG. 10. Spectral rigidity for the midenergy even-parity levels of the SES scheme from [31]. The error bars display the standard deviation of the binning process. The theory curves for Poissonian, GOE, 2GOE, and 3GOE statistics are given as gray lines. The inset comprises the residuals of the CNNSD for the fitted Brody convolution (red dashed line) and the fitted Abul-Magd distribution (blue solid line).

the even spectrum is not significant and is thus only discussed in Appendix A.

Within the superimposed odd-parity spectrum, we analyzed a total of 217 levels. Figure 9 shows the results of this analysis. The parameters of the Abul-Magd function and the composition of three Brody functions of $f = 0.33(9)$ and $\eta = 1.45(49)$, respectively, predict 3GOE level statistics of these energetically low-lying energy levels. However, the MLH fit somewhat overestimated the Brody parameter. This is probably caused by the midsize level spacings, where both functions have problems to fit the data as visible in the residual plot of the CNNSD in the inset of Fig. 9. The spectral rigidity $\Delta_3(L)$ perfectly coincides with the 3GOE curve up to correlation lengths of about $L = 4.5$, which is comparable to the correlation length of the simulated data as analyzed in Fig. 4.

From these level statistics we learn two important things.

(i) The analyzed level sequence tabulated in [33] shows no apparently missing levels. This seems to be the fact also for the case of the even-parity levels analyzed in Appendix A.

(ii) Already at these very low energies (the spectrum reaches from 0.8 to 3.7 eV) the level fluctuations are not distinguishable anymore from 3GOE statistics, at least within the correlation lengths mentioned above.

Especially the second point is remarkable, as it affects a detailed investigation of the transition region into the chaotic regime. As pointed out in Sec. I, regularity and intrinsic quantum chaos are coexisting in a specific energy region until the chaotic behavior finally becomes prevalent above. In order to analyze the spectral statistics in this region, the spectrum has to be divided into several parts which need to be analyzed separately. Unfortunately, the transition is apparently located at such low excitation energies that the number of levels in the individual parts of the spectrum is too low to extract statistically significant information on the spectral properties of this region.

B. The SES scheme

In the following we discuss the spectral statistics of three representative spectra of even-parity levels identified in Ref. [31], covering different energy ranges and both types of missing levels; an example of spectral statistics for odd-parity levels is additionally given in Appendix B. The spectrum of the SES scheme of [31], also shown in Fig. 1, covers a medium-energy range around 4.5 eV. Since excitation starts from an excited level with $J = \frac{11}{2}$, the detected levels may have values for total angular momentum in the range $J = \frac{9}{2}, \ldots, \frac{13}{2}$. With 28 energy levels this spectrum constitutes the shortest level sequence evaluated here and thus suffers from low statistical significance, which also results in very large uncertainties. Nonetheless, the analysis of the observables for level fluctuations, as comprised in Fig. 10, reveals spectral statistical properties that can be well understood if missing levels are taken into account. Already the η and f parameters of the CNNSD, $\eta = 1.46(103)$ and $f = 0.58(29)$, respectively, predict an overestimation of chaotic behavior which would be caused by missing levels of one specific submanifold, even though the large residuals as shown on the inset of Fig. 10 suffer by the low statistical significance. Comparing the data in Fig. 10 with the curves in Figs. 7 and 8, one can estimate that a very high percentage of one J manifold of more than 80% must be missing due to the J suppression discussed in Sec. III C. Most important for the SES scheme is that the data clearly deviate from nonchaotic Poissonian behavior, which testifies again to the presence of IQC in the protactinium atom already at low excitation energies.

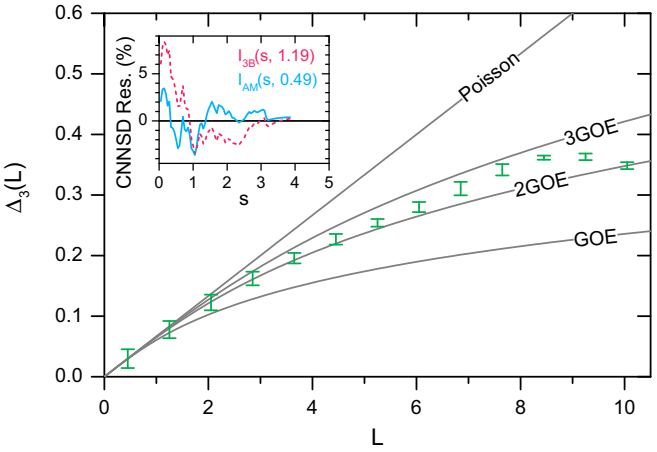

FIG. 11. Spectral rigidity for the high-energy even-parity levels of scheme (iii) from [31]. The error bars display the standard deviation of the binning process. The theory curves for Poissonian, GOE, 2GOE, and 3GOE statistics are given as gray lines. The inset comprises the residuals of the CNNSD for the fitted Brody convolution (red dashed line) and the fitted Abul-Magd distribution (blue solid line).

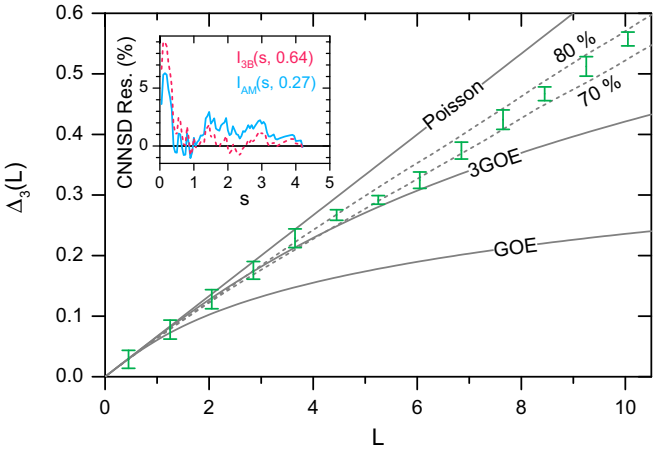

FIG. 12. Spectral rigidity for the high-energy even-parity levels of scheme (vi) from [31]. The error bars display the standard deviation of the binning process. The theory curves for Poissonian, GOE, and 3GOE statistics are given as gray solid lines. Additionally, the curves for 70% and 80% of missing levels regardless of their total angular momentum are included as gray dashed lines. The inset comprises the residuals of the CNNSD for the fitted Brody convolution (red dashed line) and the fitted Abul-Magd distribution (blue solid line). For more information see the text.

C. Scheme (iii)

The spectrum of excitation scheme (iii) in [31] with a total of 226 spectrally investigated energy levels involving total angular momenta of $J = \frac{9}{2}, \ldots, \frac{13}{2}$ is much more significant in terms of statistics. The spectral properties of this scheme covering high-energy regions just below the ionization potential are summarized in Fig. 11. The spectral rigidity follows the curve for 2GOE similarly to the SES midenergy scheme up to correlation lengths around $L = 5$. For higher L the spectral rigidity starts to slowly fluctuate between the curves for 2GOE and 3GOE. Regarding the inset of Fig. 11, the CNNSD is well described by the fitted distributions with $\eta = 1.19(44)$ and $f = 0.49(10)$, also predicting a slight overestimation of the GOE behavior of each involved J subset. Only for the smallest spacings, the residuals are somewhat larger, which can be explained by missing levels. Once again, the observables for the CNNSD and $\Delta_3(L)$ clearly deviate from Poissonian statistics consistently exhibiting an overestimation of GOE statistics due to suppression of transitions leading into levels with a certain total angular momentum J.

D. Scheme (vi)

For scheme (vi) from [31] with a total of 173 analyzed energy levels also lying in an energy range just below the ionization potential and having total angular momenta of $J = \frac{9}{2}, \ldots, \frac{13}{2}$, the situation regarding the spectral properties is consistent and convincing, although it is not satisfactory for the applied spectroscopic method: Inspecting the spectral fluctuation properties in Fig. 12, the results imply a high number of missing levels in this scan, here regardless of J. A Brody parameter of $\eta = 0.64(28)$ and an Abul-Magd parameter of $f = 0.27(11)$ already suggest a percentage of more than 30%−40% missing levels if compared to Fig. 6. In addition, the residuals depicted on the inset of Fig. 12 show strong deviation of both fitted distribution only for very small spacings, which is also clearly provoked by missing levels. The result for $\Delta_3(L)$ in Fig. 12 lies exactly between the two gray dashed curves for 70%−80% missing levels as evaluated in Sec. III B. The very long correlation lengths of this coincidence together with the consistency of the distribution parameters η and f, the corresponding residuals, and the evaluated spectral rigidity validates the applied methods of analysis. Despite the rather large amount of missing levels obtained in this excitation scheme (vi), a full expression of intrinsic quantum chaos seems nonetheless confirmed.

V. CONCLUSION AND OUTLOOK

We have analyzed several sets of energy levels of the protactinium atom concerning their spectral fluctuation properties. The sets are of different origins, stemming from the literature [33], calculations [34], and recent experimental data [31]. Since the experimental data were not separable into sets with only one total angular momentum J, all analyzed data, separable for J or not, were composed for incorporating the same range of J levels as the experimental data. Moreover, for the spectroscopic data, it was essential to investigate the influence of missing levels on the spectral fluctuations, which was performed accurately. Therefore, randomly levels were taken out either from the whole spectrum or only from one subspectrum of three superimposed submanifolds simulated by three GOE matrices in order to correctly simulate the experimental situations. In addition, the mathematical analysis of the statistical measures had to be customized for the special difficulty of nonseparability for the "good" numbers, or at least for the total angular momentum J.

As already suggested in [34], besides the short-range correlation of the therein investigated NNSD, $\Delta_3(L)$ clearly indicate agreement with GOE behavior. This was confirmed using the available data from the literature [33] for odd-parity

levels as well as even-parity levels with lower significance. For the experimental data recently obtained in [31], it was possible with extensive analysis of the missing level problem also to extract level statistics that coincide well with those of a composition of three independent GOE spectra. The spectral statistics for all cases studied strongly deviate from Poissonian statistics, or nonchaotic behavior, and therefore emphasize the prognosticated occurrence of IQC in the protactinium atom.

At excitation energies below 2 eV the energy levels available in the literature [33] already show chaotic level statistics. This means that the onset of chaos, or synonymously the transition point from regular to chaotic behavior, must be located at even lower energies. In such low-energy regimes, the level density is too small to extract the spectral properties of this transition region with high statistical significance. As a future prospect, one approach to account for the low number of energy levels is to combine several unfolded level sets with excitation energies centered in this region of different elements with comparable atomic properties, i.e., a similar number of open shells and active electrons.

For a quantification of the missing levels of either type, an empirical function that describes the influence of missing levels on the fluctuation laws would be the method of choice. Fitting such a function to the NNSD and the spectral rigidity of experimentally determined data sets could unveil even more details of the spectral properties of the underlying level subsets.

ACKNOWLEDGMENTS

The authors want to thank T. Guhr, F. Haake, and R. Heinke for many fruitful discussions. P.N. gratefully acknowledges the Carl-Zeiss-Stiftung, D.S. gratefully acknowledges the EU through ENSAR2 RESIST (Grant No. 654002), and A.V.V. and V.V.F. gratefully acknowledge the Australian Research Council and Gutenberg Fellowship for financial support. B.D. thanks the NSF of China for financial support under Grant No. 11775100.

APPENDIX A: SPECTRAL STATISTICS OF EVEN-PARITY LITERATURE DATA

Figure 13 shows the spectral statistics for the even-parity energy levels that can be found in the literature [33]. Even though the results are not significant due to too few levels (only 46) involved, the observables for the short-range correlation between the energy levels promise a full expression of chaos: While the parameters of the composition of three Brody functions and the Abul-Magd function of $\eta = 0.91(78)$ and $f = 0.31(21)$, respectively, are close to the ideal values of $f = \frac{1}{3}$ and $\eta = 1$ and thus already suggest GOE behavior, the spectral rigidity is more sensitive to non-GOE features. Here, similar to the short-range correlation due to their large uncertainties, also the spectral rigidity is not very conclusive, which is also confirmed by the rather large residuals in the inset of Fig. 13: Regarding small correlation lengths L, it might coincide with regular just as well as with 3GOE statistics. Only for larger L, the spectral rigidity starts to deviate more strongly from the Poissonian statistics. Despite the poor statistics, the results seem to be consistent with those for the odd-parity energy levels of [33] in Sec. IV A.

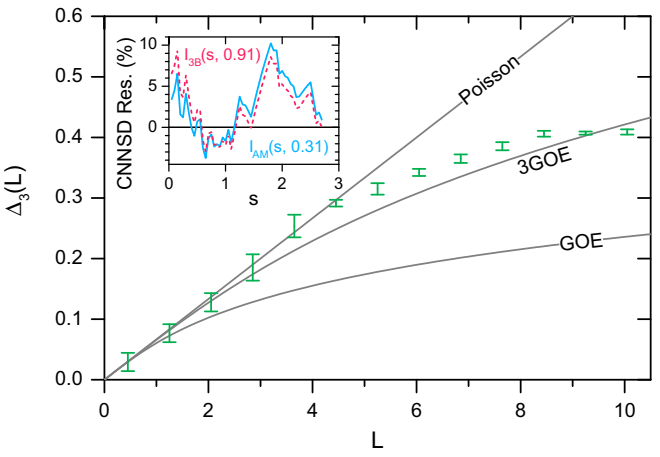

FIG. 13. Spectral rigidity for low-energy even-parity levels of [33]. The error bars display the standard deviation of the binning process. The theory curves for Poissonian, GOE, and 3GOE statistics are given as gray lines. The inset comprises the residuals of the CNNSD for the fitted Brody convolution (red dashed line) and the fitted Abul-Magd distribution (blue solid line).

APPENDIX B: SPECTRAL STATISTICS OF ODD-PARITY LEVELS FROM SCHEME (viii)

With scheme (viii) from [31], a spectrum with 168 odd-parity energy levels lying in the energy region just below the ionization potential is investigated regarding level correlations and spectral statistics. The corresponding observables for the spectral statistics, namely, the η and f parameters for fitting the CNNSD with the corresponding residuals and the spectral rigidity $\Delta_3(L)$, are comprised in Fig. 14. For the explanation of the results, the consideration of missing levels is again

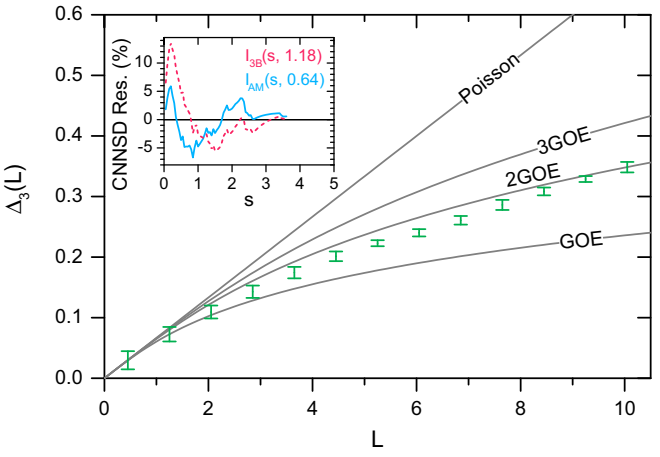

FIG. 14. Spectral rigidity for the high-energy odd-parity levels of scheme (viii) from [31]. The error bars display the standard deviation of the binning process. The theory curves for Poissonian, GOE, 2GOE, and 3GOE statistics are given as gray lines. The inset comprises the residuals of the CNNSD for the fitted Brody convolution (red dashed line) and the fitted Abul-Magd distribution (blue solid line).

mandatory. The spectral rigidity $\Delta_3(L)$ exhibits a behavior very close to the curves for 2GOE, which would be explained by the case of missing levels from only one J manifold. In addition, the results for the distribution parameters, which are with $\eta = 1.18(38)$ and $f = 0.64(13)$ close to a 2GOE behavior, testify to this overestimation of chaoticity due to the missing levels. Even though the residuals shown in the inset of Fig. 14 are at least for small spacings quite large, also here the spectral statistics clearly deviate from pure Poissonian behavior and therefore also these data seem to prove the quantum chaotical behavior of the protactinium atom.

[1] D. Delande, in *Chaos and Quantum Physics*, edited by M.-J. Giannoni, A. Voros, and J. Zinn-Justin, Proceedings of the Les Houches Summer School of Theoretical Physics, LII, Varenna, 1989 (North-Holland, Amsterdam, 1991).

[2] A. Holle, J. Main, G. Wiebusch, H. Rottke, and K. H. Welge, Phys. Rev. Lett. **61**, 161 (1988).

[3] H.-J. Stöckmann and J. Stein, Phys. Rev. Lett. **64**, 2215 (1990).

[4] H.-D. Gräf, H. L. Harney, H. Lengeler, C. H. Lewenkopf, C. Rangacharyulu, A. Richter, P. Schardt, and H. A. Weidenmüller, Phys. Rev. Lett. **69**, 1296 (1992).

[5] B. E. Sauer, M. R. W. Bellermann, and P. M. Koch, Phys. Rev. Lett. **68**, 1633 (1992).

[6] J. C. Robinson, C. Bharucha, F. L. Moore, R. Jahnke, G. A. Georgakis, Q. Niu, M. G. Raizen, and B. Sundaram, Phys. Rev. Lett. **74**, 3963 (1995).

[7] A. Buchleitner, D. Delande, J. Zakrzewski, R. N. Mantegna, M. Arndt, and H. Walther, Phys. Rev. Lett. **75**, 3818 (1995).

[8] H. Held, J. Schlichter, G. Raithel, and H. Walther, Europhys. Lett. **43**, 392 (1998).

[9] M. B. d'Arcy, R. M. Godun, M. K. Oberthaler, D. Cassettari, and G. S. Summy, Phys. Rev. Lett. **87**, 074102 (2001).

[10] S. Urazhdin, P. Tabor, V. Tiberkevich, and A. Slavin, Phys. Rev. Lett. **105**, 104101 (2010).

[11] K. Karremans, W. Vassen, and W. Hogervorst, Phys. Rev. Lett. **81**, 4843 (1998).

[12] M. C. Gutzwiller, *Chaos in Classical and Quantum Systems* (Springer, Berlin, 1990).

[13] J. von Milczewski, G. H. F. Diercksen, and T. Uzer, Phys. Rev. Lett. **73**, 2428 (1994); **76**, 2890 (1996).

[14] P. Schlagheck and A. Buchleitner, Physica D **131**, 110 (1999).

[15] N. N. Choi, M.-H. Lee, and G. Tanner, Phys. Rev. Lett. **93**, 054302 (2004).

[16] D. M. Basko, I. L. Aleiner, and B. L. Altshuler, Ann. Phys. (NY) **321**, 1126 (2006).

[17] *Many-Body Localization*, edited by J. H. Bardarson, F. Pollmann, U. Schneider, and S. Soudhi, special issue of Ann. Phys. (Berlin) **529**(7), 1700191 (2017).

[18] R. U. Haq, A. Pandey, and O. Bohigas, Phys. Rev. Lett. **48**, 1086 (1982).

[19] H. Alt, C. Dembowski, H.-D. Gräf, R. Hofferbert, H. Rehfeld, A. Richter, R. Schuhmann, and T. Weiland, Phys. Rev. Lett. **79**, 1026 (1997).

[20] T. Maier, H. Kadau, M. Schmitt, M. Wenzel, I. Ferrier-Barbut, T. Pfau, A. Frisch, S. Baier, K. Aikawa, L. Chomaz, M. J. Mark, F. Ferlaino, C. Makrides, E. Tiesinga, A. Petrov, and S. Kotochigova, Phys. Rev. X **5**, 041029 (2015).

[21] J. Madroñero and A. Buchleitner, Phys. Rev. Lett. **95**, 263601 (2005).

[22] G. Stania and H. Walther, Phys. Rev. Lett. **95**, 194101 (2005).

[23] L. Muñoz, R. A. Molina, J. M. G. Gómez, and A. Heusler, Phys. Rev. C **95**, 014317 (2017).

[24] B. Dietz, A. Heusler, K. H. Maier, A. Richter, and B. A. Brown, Phys. Rev. Lett. **118**, 012501 (2017).

[25] R. Püttner, B. Grémaud, D. Delande, M. Domke, M. Martins, A. S. Schlachter, and G. Kaindl, Phys. Rev. Lett. **86**, 3747 (2001).

[26] Y. H. Jiang, R. Püttner, D. Delande, M. Martins, and G. Kaindl, Phys. Rev. A **78**, 021401 (2008).

[27] H. Held and W. Schweizer, Phys. Rev. Lett. **84**, 1160 (2000).

[28] N. Rosenzweig and C. E. Porter, Phys. Rev. **120**, 1698 (1960).

[29] H. S. Camarda and P. D. Georgopulos, Phys. Rev. Lett. **50**, 492 (1983).

[30] V. V. Flambaum, A. A. Gribakina, G. F. Gribakin, and M. G. Kozlov, Phys. Rev. A **50**, 267 (1994).

[31] P. Naubereit, T. Gottwald, D. Studer, and K. Wendt, preceding paper, Phys. Rev. A **98**, 022505 (2018).

[32] O. Bohigas, M. J. Giannoni, and C. Schmit, Phys. Rev. Lett. **52**, 1 (1984).

[33] J. Blaise and J.-F. Wyart, *Energy Levels and Atomic Spectra of Actinides*, available at http://web2.lac.u-psud.fr/lac/Database/Contents.html (accessed 20 March 2018) (TIC, Paris, 1992).

[34] A. V. Viatkina, M. G. Kozlov, and V. V. Flambaum, Phys. Rev. A **95**, 022503 (2017).

[35] K. Wendt, T. Gottwald, C. Mattolat, and S. Raeder, Hyperfine Interact. **227**, 55 (2014).

[36] A. A. Gribakina, and G. F. Gribakin, J. Phys. B **29**, L809 (1996).

[37] F. Haake, *Quantum Signatures of Chaos*, Springer Series in Synergetics Vol. 54 (Springer, Berlin, 2013).

[38] T. Guhr, A. Müller-Groeling, and H. A. Weidenmüller, Phys. Rep. **299**, 189 (1998).

[39] F. J. Dyson and M. L. Mehta, J. Math. Phys. **4**, 701 (1963).

[40] T. A. Brody, Lett. Nuovo Cimento **7**, 482 (1973).

[41] A. Y. Abul-Magd and M. H. Simbel, Phys. Rev. C **54**, 1675 (1996).

[42] M. A. Jafarizadeh, N. Fouladi, H. Sabri, and B. Rashidian Maleki, Nucl. Phys. A **890-891**, 29 (2012).

[43] M. L. Mehta, *Random Matrices* (Academic, New York, 2004), Vol. 142.

[44] O. Bohigas and M. P. Pato, Phys. Lett. B **595**, 171 (2004).